受入
92-12-890
高工研図書室

EUROPEAN ORGANIZATION FOR NUCLEAR RESEARCH

CERN-PPE / 92 - 169
October 1, 1992

MEASUREMENT OF THE GLUON STRUCTURE FUNCTION FROM DIRECT PHOTON DATA AT THE CERN $\bar{p}p$ COLLIDER

The UA2 Collaboration

Bern - Cambridge - CERN - Dortmund - Heidelberg - Melbourne -
Milano - Orsay (LAL) - Pavia - Perugia - Pisa - Saclay (CEN)

J.Alitti[12], G.Ambrosini[9], R.Ansari[8], D.Autiero[11], P.Bareyre[12], I.A.Bertram[6], G.Blaylock[3,a], P.Bonamy[12], K.Borer[1], M.Bourliaud[12], D.Buskulic[8], G.Carboni[11], D.Cavalli[7], V.Cavasinni[11], P.Cenci[10], J.C.Chollet[8], C.Conta[9], G.Costa[7], F.Costantini[11], L.Cozzi[7], A.Cravero[7], M.Curatolo[11], A.Dell'Acqua[3,9], T.DelPrete[11], R.S.DeWolf[2], L.DiLella[3], Y.Ducros[12], G.F.Egan[6], K.F.Einsweiler[3,b], B.Esposito[11], L.Fayard[8], A.Federspiel[1], R.Ferrari[9], M.Fraternali[9], D.Froidevaux[3], G.Fumagalli[9], J.M.Gaillard[8,3], F.Gianotti[7], O.Gildemeister[3], C.Gössling[4], V.G.Goggi[9], S.Grünendahl[5], K.Hara[1,c], S.Hellman[3], J.Hrivnac[3,d], H.Hufnagel[4], E.Hugentobler[1], K.Hultqvist[3,e], E.Iacopini[11,f], J.Incandela[7,g], K.Jakobs[3,h], P.Jenni[3], E.E.Kluge[5], N.Kurz[5], S.Lami[11], P.Lariccia[10], M.Lefebvre[3,i], L.Linssen[3], M.Livan[9], P.Lubrano[3,10], C.Magneville[12], L.Malgeri[j], L.Mandelli[7], L.Mapelli[3], M.Mazzanti[7], K.Meier[3,k], B.Merkel[8], J.P.Meyer[12], M.Moniez[8], R.Moning[1], M.Morganti[11], L.Müller[1], D.J.Munday[2], M.Nessi[3], F.Nessi-Tedaldi[3,l], C.Onions[3], T.Pal[1,m], M.A.Parker[2], G.Parrour[8], F.Pastore[9], E.Pennacchio[9], J.M.Pentney[3,n], M.Pepe[3], L.Perini[7], C.Petridou[11,o], P.Petroff[8], H.Plothow-Besch[3], G.Polesello[9], A.Poppleton[3], K.Pretzl[1], M.Primavera[11,j], M.Punturo[10], J.P.Repellin[8], A.Rimoldi[9], M.Sacchi[9], P.Scampoli[10], J.Schacher[1], B.Schmidt[4], V.Simak[3,d], S.L.Singh[2], V.Sondermann[4], R.Spiwoks[4], S.Stapnes[3,p], C.Talamonti[10], F.Tondini[10], S.N.Tovey[6], E.Tsesmelis[4], G.Unal[8], M.Valdata-Nappi[11,j], V.Vercesi[9], A.R.Weidberg[3,q], P.S.Wells[2,r], T.O.White[2], D.R.Wood[8,g], S.A.Wotton[2,r], H.Zaccone[12], A.Zylberstejn[12]

(Submitted to Physics Letters B)

ABSTRACT

A measurement of the gluon structure function using direct photon events observed with the UA2 detector in $\bar{p}p$ collisions at $\sqrt{s} = 630$ GeV is presented. The x-range covered by this analysis is between 0.049 and 0.207 and the Q^2 range is between 280 GeV^2 and 3670 GeV^2. The data sample corresponds to an integrated luminosity of 7.14 pb^{-1}. The results are found to be in good agreement with the gluon distributions measured in deep inelastic scattering experiments extrapolated to the UA2 Q^2 values.

1 Laboratorium für Hochenergiephysik, Universität Bern, Sidlerstraβe 5, 3012 Bern, Switzerland
2 Cavendish Laboratory, University of Cambridge, Cambridge, CB3 0HE, UK
3 CERN, 1211 Geneva 23, Switzerland
4 Lehrstuhl für Exp. Physik IV, Universität Dortmund, 4600 Dortmund, Germany
5 Institut für Hochenergiephysik Universität Heidelberg, Schröderstraβe 90, 6900 Heidelberg, Germany
6 School of Physics, University of Melbourne, Parkville 3052, Australia.
7 Dipartimento di Fisica dell'Università di Milano and Sezione INFN Milano, 20133 Milano, Italy
8 Laboratoire de l'Accélérateur Linéaire, Université de Paris-Sud, 91405 Orsay, France
9 Dipartimento di Fisica Nucleare e Teorica, Università di Pavia and INFN, Sezione di Pavia, Via Bassi 6, 27100 Pavia, Italy
10 Dipartimento di Fisica dell'Università di Perugia and INFN, Sezione di Perugia, via Pascoli, 06100 Perugia, Italy
11 Dipartimento di Fisica dell'Università di Pisa and INFN, Sezione di Pisa, Via Livornese, S.Piero a Grado, 56100 Pisa, Italy
12 Centre d'Etudes Nucléaires de Saclay, 91191 Gif-sur-Yvette Cedex, France

a) Now at University of California, Santa Cruz, California, USA
b) Now at Lawrence Berkeley Laboratory, Berkeley, California, USA
c) Now at University of Tsukuba, Tsukuba, Ibaraki 305, Japan
d) Now at Institute of Physics, CSAV, Praha 8, Czechoslovakia
e) Now at University of Stockholm, Stockholm, Sweden
f) Also at Scuola Normale Superiore, Pisa, Italy
g) Now at Fermi National Accelerator Laboratory, Batavia, Illinois, USA
h) Now at Max Planck Institut für Physik, D 8000 München, Germany
i) Now at University of Victoria, Victoria, Canada
j) Now at Dipartimento di Fisica dell'Università della Calabria e gruppo INFN, Cosenza, Italy
k) Now at Deutsches Elektronen Synchrotron, Hamburg, Germany
l) Now at Eidgenössische Technische Hochschule, ETH Zürich, CH 8093 Zürich, Switzerland
m) Now at SSCL, 2550 Beckleymeade Av., Dallas, Texas, USA
n) Now at Department of Physics, Brunel University, Uxbridge, London, UK
o) Now at INFN Sezione di Trieste, Laboratori Area di Ricerca, Padriciano 99, 34012 Trieste, Italy
p) Now at Physics Institute, University of Oslo, Blindern, Oslo, Norway
q) Now at Nuclear Physics Laboratory, University of Oxford, Oxford, UK
r) Now at CERN, Geneva, Switzerland.

1. INTRODUCTION

Deep inelastic lepton-nucleon scattering data have been extensively used to determine the gluon momentum distribution inside protons and nuclei [1]. Since gluons do not couple to a lepton probe, these results are obtained only in an indirect way making use of the scaling violation of quark structure functions. A more direct method of determining the gluon momentum distribution is through the study of prompt photon production in hadron collisions.

In this analysis the gluon structure function $G(x,Q^2)$ has been determined in the range $0.049 \leq x \leq 0.207$ and $280\ GeV^2 < Q^2 < 3670\ GeV^2$, by measuring both the photon and the recoiling jet, and using the known quark distribution functions and lowest order parton-parton QCD cross-sections. The measurement has been performed using a data sample collected during the 1988 and 1989 UA2 runs, corresponding to an integrated luminosity of $7.14\ pb^{-1}$. A similar study, in the x-range between 0.15 and 0.30, was reported for proton-proton interactions at $\sqrt{s} = 63$ GeV [2].

This paper is organized as follows: Section 2 describes the parts of the UA2 detector relevant for this analysis, while Section 3 outlines the dynamical description of prompt photon production. The data reduction and the angular acceptance are discussed in Section 4. The method used to extract the gluon structure function and the comparison with the theoretical predictions are described in Section 5. Finally, the systematic uncertainties on the measurement are discussed in Section 6.

2. THE UA2 APPARATUS

The UA2 detector [3], which provides full calorimetric coverage around the interaction region in the pseudorapidity range $-3 < \eta < 3$, consists of a central tracking detector surrounded by electromagnetic and hadronic calorimeters [4]. The calorimeter is divided into a central part (CC) within $|\eta| < 1$ and two end cap regions (EC) reaching $|\eta| = 3$. All calorimeters use the sampling technique, with a tower structure and wavelength shifter readout. The granularity is $\Delta\theta \cdot \Delta\phi = 10^\circ \cdot 15^\circ$ in the CC and $\Delta\eta \cdot \Delta\phi = 0.2 \cdot 15^\circ$ in the EC, except for the two cells closest to the beam axis which have $\Delta\eta = 0.3$ and 0.5 respectively. The electromagnetic compartments are multi-layer lead-scintillator sandwiches with a total thickness of 17 radiation lengths (r.l.) in the CC and varying between 17.1 and 24.4 r.l. in the EC, depending on the polar angle θ. The hadronic compartments are multi-layer iron-scintillator sandwiches, 4 absorption lengths (a.l.) deep in the CC and 6.5 a.l. deep in the EC.

Clusters are reconstructed in the calorimeter by joining all cells with an energy greater than 400 MeV sharing a common edge. Clusters with a small lateral size and a small energy leakage into the hadronic compartments are marked as electromagnetic clusters.

The central detector, used to determine the position of the event vertex and to reconstruct charged particle tracks, consists of two silicon pad counter arrays [5] around the beam at radii of 2.9 cm and 14.8 cm. A cylindrical drift chamber [6] is located between the two silicon detectors. Beyond the outer silicon layer there is a transition radiation detector [7], consisting of two sets of radiators and proportional chambers, followed by a scintillating fibre detector [8] which provides track segments in the first six stereo triplets of fibres and localizes the beginning of electromagnetic showers in front of the CC in the last two stereo triplets, located after a 1.5 r.l. thick lead converter.

In the forward regions, $|\eta| > 1$, tracking and preshower measurements are provided by three stereo triplets of proportional tubes [9] placed in front of the EC. The first two triplets are used as a tracking device, while the last triplet, placed after a 2 r.l. thick iron and lead converter, acts as a preshower detector. Two sets of time-of-flight hodoscopes are located at small angles with respect to the beam. Their function is to define a minimum bias trigger and to provide an independent vertex measurement. Finally, two planes of large area scintillation counters cover the back of the EC. Events caused by beam halo particles are rejected in the analysis by detecting charged particles giving an early signal in these counters with respect to the beam crossing time.

3. PROMPT PHOTON PRODUCTION

At the lowest order in α_s direct photons are produced through two elementary processes: Compton scattering ($gq \rightarrow \gamma q$) and annihilation ($\bar{q}q \rightarrow \gamma g$) [10]. The differential cross-sections at parton level are respectively:

$$\frac{d\hat{\sigma}^C}{d\hat{t}} = \frac{2}{\hat{s}} \frac{d\hat{\sigma}^C}{d\cos\theta^*} = \pi \alpha \alpha_s e_q^2 \left(-\frac{1}{3\hat{s}^2}\right)\left(\frac{\hat{u}}{\hat{s}} + \frac{\hat{s}}{\hat{u}}\right) \equiv \pi \alpha \alpha_s e_q^2 W^C(\hat{s},\hat{t},\hat{u}) \qquad (1)$$

$$\frac{d\hat{\sigma}^A}{d\hat{t}} = \frac{2}{\hat{s}} \frac{d\hat{\sigma}^A}{d\cos\theta^*} = \pi \alpha \alpha_s e_q^2 \left(\frac{8}{9\hat{s}^2}\right)\left(\frac{\hat{u}}{\hat{t}} + \frac{\hat{t}}{\hat{u}}\right) \equiv \pi \alpha \alpha_s e_q^2 W^A(\hat{s},\hat{t},\hat{u}) \qquad (2)$$

where $\hat{s}$, $\hat{t}$ and $\hat{u}$ are the Mandelstam variables for the parton-parton scattering *ab* -> *cd*. These variables and the functions $W^{A(C)}$ can be expressed through the fractions (x_1,x_2) of the longitudinal hadron momenta carried by the two colliding partons and the parton center of mass scattering angle (θ^*). The differential cross-section for the production of a prompt photon and a jet in proton-antiproton collisions becomes [11]:

$$\frac{d^3\sigma}{dx_1\,dx_2\,d\cos\theta^*} = \frac{d^3\sigma^A}{dx_1\,dx_2\,d\cos\theta^*} + \frac{d^3\sigma^C}{dx_1\,dx_2\,d\cos\theta^*} =$$

$$= \frac{x_1 x_2 s}{2}\left[\frac{d^3\sigma^A}{dx_1\,dx_2\,d\hat{t}} + \frac{d^3\sigma^C}{dx_1\,dx_2\,d\hat{t}}\right] \qquad (3)$$

where s is the center of mass energy squared.

Each term $\frac{d^3\sigma^{A(C)}}{dx_1\,dx_2\,d\hat{t}}$ can be factorized into two parts, one containing the parton density functions and the other containing the elementary cross-sections (1) and (2). The resulting total cross section integrated over $\cos\theta^*$ is:

$$\frac{d^2\sigma}{dx_1 dx_2} = \frac{\pi\alpha}{x_1 x_2}\left[\sum_i f^i(x_1,Q^2) f^i(x_2,Q^2)\int_{-\cos\theta^*_{max}}^{\cos\theta^*_{max}} \alpha_S W^A(\cos\theta^*)\,d\cos\theta^* + \right.$$

$$\left.\left(G(x_1,Q^2)\sum_i f^i(x_2,Q^2) + G(x_2,Q^2)\sum_i f^i(x_1,Q^2)\right)\int_{-\cos\theta^*_{max}}^{\cos\theta^*_{max}} \alpha_S W^C(\cos\theta^*)\,d\cos\theta^*\right] \qquad (4)$$

where $\cos\theta^*_{max}$ is the maximum $\cos\theta^*$ value accessible by the UA2 apparatus.

In this expression $f^i(x,Q^2)$ are the distribution functions of the different quark flavours in the proton multiplied by the square of the quark electric charge, and $G(x,Q^2)$ is the gluon structure function . It is important to note that $G(x,Q^2)$ is the only unknown function: it can be extracted, therefore, by measuring $d^2\sigma$ (γ+jet) / $dx_1 \cdot dx_2$ and comparing the results with the theoretical formula (4). We note that the approximation made in taking the structure function terms out of the integral is

reasonable since Q^2 varies by at most a factor of 2 over the $\cos\theta^*$ interval accessible here.

4. EVENT SELECTION AND ANGULAR ACCEPTANCE

4.1 DATA REDUCTION

The events are selected by requiring a reconstructed vertex within ± 250 mm of the detector centre along the beam axis, and the presence of one electromagnetic cluster. A photon candidate is defined as an electromagnetic cluster satisfying the following criteria:

- $p_T > 15$ GeV and $|\eta| < 0.76$, where the pseudorapidity η is calculated from the centre of the UA2 apparatus.

- Lateral and longitudinal profiles of the cluster consistent with that expected from a single isolated electron or photon as determined from test beam data.

- The absence of charged tracks in front of the calorimeter cluster, as required by pulse height cuts on all silicon pads within a window of $\Delta\eta < 0.2$ and $\Delta\phi < 15^\circ$ about the cluster axis (defined by the line joining the interaction vertex to the cluster centroid).

- At most one preshower signal in a cone $\sqrt{\Delta\phi^2 + \Delta\eta^2} < 0.265$ about the cluster axis.

The track isolation cut suppresses most of the π^0 background and also photons from bremsstrahlung of final state quarks.

Jets recoiling against the prompt photon candidate are sought in events containing at least one hadronic cluster with the highest transverse energy E_T exceeding 5 GeV. Final state gluon radiation is taken into account by adding vectorially any additional clusters in the event with $E_T > 3$ GeV and with an angular separation ω from the leading cluster axis such that $\cos\omega > 0.2$ [12]. The γ-jet sample is then selected by the following conditions:

- $p_T(jet) > 10$ GeV , $|\eta_{jet}| < 2$.

- Azimuthal separation between the photon and the jet directions

  $\Delta\phi(\gamma\text{-jet}) > 120^\circ$.

- No other jet in the event exceeding $E_T > 6$ GeV. This cut rejects photon bremsstrahlung and jets coming from initial state gluon radiation.

A total of 13574 γ-jet candidates satisfy these criteria.

4.2 ANGULAR DISTRIBUTION

The center of mass scattering angle θ^* is defined following the Collins-Soper convention [13] . The angular acceptance is studied by considering the event distribution in the $\cos\theta^*$-$\beta_{\gamma\text{-jet}}$ plane , where $\beta_{\gamma\text{-jet}}$ is the velocity of the γ-jet system in the laboratory frame. For the selected γ-jet candidates the calorimeter acceptance is uniform in a well defined domain of this plane, R*, which depends for each event on the interaction vertex position along the beam axis (z_v). If a γ-jet candidate has coordinates in the $\cos\theta^*$-$\beta_{\gamma\text{-jet}}$ plane outside this $R^*(z_v)$ domain, the event is rejected.

A total of 5525 events survive this selection. Their distribution in the $\cos\theta^*$-$\beta_{\gamma\text{-jet}}$ plane is shown in Fig.1, corresponding to the convolution of all the $R^*(z_v)$ regions involved .

For each event, x_1 and x_2 are computed from the following relations:

$$\frac{2\, p_L^{(\gamma+\text{jet})}}{\sqrt{s}} = x_1 - x_2$$
$$m^2_{(\gamma+\text{jet})} = s\, x_1\, x_2 \qquad (5)$$

The distribution of x_1 (x_2) is shown in Fig. 2.

For a given vertex position every (x_1,x_2) pair defines unambiguously $\cos\theta^*_{max}$ which is the maximum value of $\cos\theta^*$ detectable with uniform acceptance. This value sets the integration limit in formula (4). Each $\cos\theta^*_{max}$ (x_1, x_2, z_v) defines a point on the boundary of the region $R^*(z_v)$ in the $\beta_{\gamma\text{-jet}}$ - $\cos\theta^*$ plane.

Due to the difficulty in performing the integration (4) with a $\cos\theta^*_{max}$ value which is different event by event depending on the vertex position, five functions $\cos\theta^{*i}_{max}$ (x_1, x_2) (i = 1,..,5) have been computed, corresponding to $\cos\theta^*_{max}$ values relative to five vertex positions, namely z_v = -200 , -100 , 0 , 100 , 200 mm. The effect introduced by approximating the convolution of all the $R^*(z_v)$ regions with the convolution of $R^*(z_v^i)$ is found to be negligible.

5. GLUON STRUCTURE FUNCTION DETERMINATION AND COMPARISON WITH THEORETICAL PREDICTIONS

5.1 EXPERIMENTAL PHOTON-JET CROSS SECTION $\frac{d^2\sigma(\gamma+jet)}{dx_1 dx_2}$

The γ - jet events selected in the R* regions of uniform angular acceptance of the central calorimeter have been arranged into an (x_1,x_2) matrix. The events falling in each $(\Delta x_1 \cdot \Delta x_2)$ domain are distributed over five intervals of z_v centered on the above values with a width of 100 mm.

The contamination $b(E_\gamma)$ of the residual π^0 and η background in the γ - jet sample has been subtracted on a statistical basis as described in ref [14]. Every γ - jet event has been weighted with the factor $[1 - b(E_\gamma)]$ and the experimental differential cross section $d^2\sigma / dx_1\, dx_2$ has been computed for the five z_v regions, using for each of them the luminosity values:

$$\left[\int L dt\right]^i = F_v^i \int L dt$$

where $\int L dt = 7.14 \pm 0.55$ pb^{-1} is the integrated luminosity corresponding to the 1988-1989 data sample and F_v^i is the fraction of events contained in the i-th z_v interval.

The five cross sections $d^2\sigma_i / dx_1\, dx_2$ have been added together to obtain an experimental quantity $S^*(x_1,x_2)$ defined as:

$$S^*(x_1,x_2) = \sum_{i=1}^{5} \frac{d^2\sigma_i}{dx_1 dx_2} = \frac{C(x_1,x_2)}{\Delta x_1 \Delta x_2\, \varepsilon_c} \sum_{i=1}^{5} \frac{N^*(x_1,x_2,z^i_v)}{\varepsilon_{\gamma j} \left[\int L dt\right]^i} \qquad (6)$$

where $N^*(x_1,x_2,z_v^i)$ is the number of γ - jet events after the statistical subtraction of the background in the $(\Delta x_1 \cdot \Delta x_2)$ bin of area $\Delta x_1 \Delta x_2$, ε_c is the direct photon global detection efficiency [14], $\varepsilon_{\gamma j}$ is the efficiency of the selection criteria applied to obtain the γ - jet sample. The quantity $C(x_1,x_2)$, generally equal to 1, corrects for the fact that not all the z_v^i bins contribute to a given $(\Delta x_1 \cdot \Delta x_2)$ bin.

The γ - jet selection efficiency $\varepsilon_{\gamma j}$ has been computed by a Monte Carlo simulation which generates prompt photon + jet events to the lowest order [15] and uses the full UA2 calorimeter modelling. This efficiency has been found to be independent of x for the most of the $(\Delta x_1 \cdot \Delta x_2)$ domain considered in the analysis, except for few bins of (x_1, x_2) in the lowest x-region.

5.2 DETERMINATION OF $G(x,Q^2)$

The gluon structure function is determined by solving the system of linear equations

$$S^*(x_1,x_2) = S^{th}(x_1,x_2) \qquad (7)$$

in which $G(x_1,Q^2)$ and $G(x_2,Q^2)$ are the unknowns and $S^{th}(x_1,x_2)$ is defined as the sum of the five cross sections $d^2\sigma_i / dx_1\, dx_2$ computed using equation (4) where, for each z_v bin, the relevant $\cos\theta^*_{max}$ value is used. The Q^2 scale is chosen equal to p_T^2 and $\alpha_s = 12\pi / [23 \ln (Q^2/\Lambda^2_{QCD})]$.

Different sets of parametrizations of the quark density functions $f^i(x,Q^2)$ are used [16]: Duke-Owens set 1.1 [17], DFLM (with Λ_{QCD} = 160 MeV) [18], HMRSB (with Λ_{QCD} = 190 MeV) [19], KMRS set B0 (with Λ_{QCD} = 190 MeV) [20], Morfin-Tung set S1 [21].

Two different methods are used to determine $G(x,Q^2)$.

In the first, $G(x,Q^2)$ has been computed by solving system (7) in seven x-bins covering the region $0.049 < x < 0.207$ in the case where x_1 and x_2 fall in the same x bin. The results of this method are given in Table 1 and shown if Fig. 3a) where the structure functions of ref. [21] have been chosen to parametrize the quark density distributions.

In the second method a global fit of $S^*(x_1,x_2)$ to $S^{th}(x_1,x_2)$ has been performed. This method can only be applied if one neglects the Q^2 dependence of the G values because each equation (7) refers to a different Q^2 value. Table 2 lists the values of the gluon structure function obtained when the global fit procedure is applied using the same quark density distributions as in the first method. The results are presented in Fig. 3b). In this case the theoretical gluon parametrization is computed at the average Q^2 measured from the data: $\langle Q^2 \rangle = 417$ GeV^2.

Table 1: Gluon structure function measured for $x_1 = x_2$

<x>	$<Q^2>$	$G(x,Q^2)$	$\Delta G(x,Q^2)$ (stat.)	$\Delta G(x,Q^2)$ (syst.)	$\Delta G(x,Q^2)$ (tot.)
0.049	280.48	3.053	0.165	0.580	0.603
0.069	414.66	2.120	0.184	0.424	0.462
0.089	743.45	1.298	0.274	0.293	0.401
0.108	1069.11	0.882	0.389	0.231	0.452
0.129	1443.52	0.637	0.605	0.207	0.639
0.155	2106.56	0.024	0.276	0.102	0.294
0.207	3665.98	0.394	0.573	0.162	0.595

Table 2: Gluon structure function measured whit a global fit procedure

<x>	G(x)	$\Delta G(x)$
0.049	2.859	0.381
0.069	1.969	0.326
0.089	1.306	0.288
0.108	0.592	0.285
0.129	0.476	0.352
0.155	0.274	0.389
0.207	0.417	0.414

Both results are in good agreement with the gluon density distribution determined from deep inelastic lepton-nucleon scattering data and extrapolated to the Q^2 values accessible to this experiment.

It must be stressed that the choice of the quark structure function parametrizations [17-21] results in a variation of $G(x,Q^2)$ which is much smaller than its statistical error. This is illustrated in Fig.4a) and 4b) which show the gluon structure function obtained using the two methods described above and a different parametrization for the quark density distributions (HMRSB ref. [19]). The same applies for all the other sets of quark structure functions used in this analysis [17-21].

The systematic errors listed in Table 1 and shown in Figs. 3 and 4 are the quadratic combination of the x-dependent uncertainties coming from the luminosity

measurement, the global efficiency of the photon selection, the background fraction determination and the γ-jet selection efficiency . To estimate the latter a different Monte Carlo generation of γ–jet events [15] has been made, suppressing the quark initial state radiation and superimposing an additional minimum bias event on the γ-jet event. For this case $\varepsilon_{\gamma j}$ has been recomputed and the difference from the previous value has been taken as the systematic uncertainty on $\varepsilon_{\gamma j}$. The errors reported in Table 2 and in Fig. 3b) are the results obtained using the global fit procedure when the input errors on the cross-section data are the quadratic combinations of the statistical and of all the systematic uncertainties listed above.

Other contributions to the systematic error resulting from both theoretical and experimental uncertainties will be discussed in the next section.

6. SYSTEMATIC UNCERTAINTIES

The error on the energy scales of the electromagnetic (1%) and hadronic (2%) compartments of the calorimeter affects the photon and the jet energy measurements respectively. The systematic uncertainty ($\Delta G/G$) on the gluon structure function resulting from these errors has been computed by varying the energy scale in the data. The contribution due to the error on the γ energy measurement and that due to the uncertainty on the jet energy have been added in quadrature, resulting in a total systematic error of $\Delta G/G = 4.8\%$.

The error resulting from the differences in the energy reconstruction for converted and unconverted photons [14] gives an uncertainty of $\Delta G/G = 4.9\%$.

The uncertainty resulting from the jet reconstruction algorithm has been estimated by recomputing the gluon structure function after changing the cone algorithm as described in Ref. [22]. The uncertainty on G evaluated in this way is found to be $\Delta G/G = 15.0\%$.

Since the photon-jet cross-section depends weakly on the QCD scale parameter Λ_{QCD}, this parameter cannot be extracted from the data in an independent way. The uncertainty due to the ambiguity in the Λ_{QCD} choice has been evaluated changing the Λ_{QCD} value in α_S in the range between 150 MeV and 250 MeV. The resulting variation on $G(x,Q^2)$ is $\Delta G/G = 7.0\%$.

Finally, the Q^2 scale has been changed from $Q^2 = p_T^2$ to $Q^2 = (4/3)p_T^2$, to estimate the dependence of the gluon structure function on the Q^2 definition. This results in a relative difference of $\Delta G/G = 2.6\%$.

The total systematic uncertainty due to the sources reported in this section amounts to $\Delta G/G = 18.1\%$.

7. CONCLUSIONS

From the study of the prompt photon+jet production, a direct measurement of the gluon structure function has been obtained with the UA2 apparatus in the range $0.049 < x < 0.207$ for Q^2 values between 280 GeV^2 and 3670 GeV^2.

The results are in agreement with the parametrizations of the gluon density function extrapolated from deep inelastic neutrino-nucleon scattering data.

ACKNOWLEDGEMENTS

We especially thank P. Bagnaia for many fruitful discussions. The technical staff of the institutes collaborating in UA2 have contributed substantially to the construction and operation of the experiment. We thank them deeply for their support. The experiment would not have been possible without the very succesful operation of the improved CERN $\bar{p}p$ Collider, whose staff and coordinators we sincerely thank for their collective effort.

Financial support from the Schweizerischen Nationalfonds zur Förderung der Wissenschaftlichen Forschung to the Bern group, from the UK Science and Engineering Research Council to the Cambridge group, from the Bundesministerium für Forschung und Technologie to the Dortmund and Heidelberg groups, from the Australian Research Council, the CRA Pty Ltd, and the Victorian Education Foundation to the Melbourne group, from the Institut National de Physique Nucléaire et de Physique des Particules to the Orsay group, from the Istituto Nazionale di Fisica Nucleare to the Milano, Pavia, Perugia and Pisa groups and from the Institut de Recherche Fondamentale (CEA) to the Saclay group are acknowledged.

REFERENCES

[1] F. Bergsma et al., Phys. Lett. 123B (1983) 269;
J.J. Aubert et al., Nucl. Phys. B259 (1985) 189;
A.C. Benvenuti et al., Phys. Lett. 195B (1987) 91; Phys. Lett. 195B (1987) 97.

[2] T. Akesson et al., Soviet J. Nucl. Phys. 51 (1990) 836.

[3] UA2 Collaboration, C.N. Booth, Proc. 6th Topical Workshop on Proton-Antiproton Collider Physics (Aachen, 1986), eds. K. Eggert et al. (World Scientific, Singapore, 1987) 381.

[4] A. Beer et al., Nucl. Instrum. Methods A224 (1984) 360.

[5] R. Ansari et al., Nucl. Instrum. Methods A279 (1989) 388.

[6] F. Bosi et al., Nucl. Instrum. Methods A283 (1989) 532.

[7] R. Ansari et al., Nucl. Instrum. Methods A263 (1988) 51.

[8] R.E. Ansorge et al., Nucl. Instrum. Methods A265 (1988) 33;
J. Alitti et al., Nucl. Instrum. Methods A279 (1989) 364.

[9] K. Borer et al., Nucl. Instrum. Methods A286 (1990) 128.

[10] F. Halzen and D.M. Scott, Phys. Lett. B78 (1978) 318.

[11] J.F. Owens, Rev. Mod. Phys. 59 (1987) 465.

[12] P. Bagnaia et al., Phys. Lett. 144B(1984) 283.

[13] J.C. Collins, D.E. Soper, Phys. Rev. D16 (1977) 2219.

[14] J. Alitti et al., Phys. Lett. 263B (1991) 544.

[15] H.U. Bengtsson, T. Sjöstrand, PYTHIA, Comput. Phys. Commun. 46 (1987) 43.

[16] H. Plothow-Besch, 'Parton Density Functions', Proc. of the 3rd Workshop on Detector and Event Simulation in High Energy Physics, Amsterdam, 8-12 April 1991.

[17] J.F. Owens, FSU-HEP-910606 (1991).

[18] M. Diemoz et al., Z. Phys. C - Particle and Field 39 (1988) 21.

[19] P.N. Harriman et al., Phys. Rev. D42 (1990) 798; Phys. Lett. 243B (1990) 421.

[20] J. Kwiecinski et al., Phys. Rev. D42 (1990) 3645.

[21] J.G. Morfin, W.K. Tung, Z. Phys. C - Particle and Field 52 (1991) 13.

[22] J. Alitti et al., Phys. Lett. 257B (1991) 232.

FIGURE CAPTIONS

Fig. 1 Distribution in the $\beta_{\gamma\text{-jet}}$-cos$\theta^*$ plane of the γ-jet candidates falling in the regions (R*) of uniform angular acceptance in the calorimeter (see text).
The full line displays the boundary of the R* region computed for a vertex displacement along the beam axis of 0. mm, while the dashed and the dashed-dot lines are the boundaries for a vertex displacement along the beam axis of +100 and -100 mm respectively.

Fig. 2 Distribution of the fraction (x_1,x_2) of the longitudinal hadron momenta carried by the two colliding partons for the selected γ-jet events.

Fig. 3 (a) Comparison between the gluon structure function obtained from the data at $x_1 = x_2$ using the quark parametrizations of ref. [21] and (full line) the gluon density distribution determined from deep inelastic lepton-nucleon scattering data and extrapolated to the Q^2 values accessible to this experiment.
(b) Same as (a) when the experimental gluon structure function is obtained using the fit procedure (see text).

Fig. 4 (a) Comparison between the gluon structure function obtained from the data at $x_1 = x_2$ using the quark parametrizations of ref. [19] and (full line) the gluon density distribution determined from deep inelastic lepton-nucleon scattering data and extrapolated to the Q^2 values accessible to this experiment.
(b) Same as (a) when the experimental gluon structure function is obtained using the fit procedure (see text).

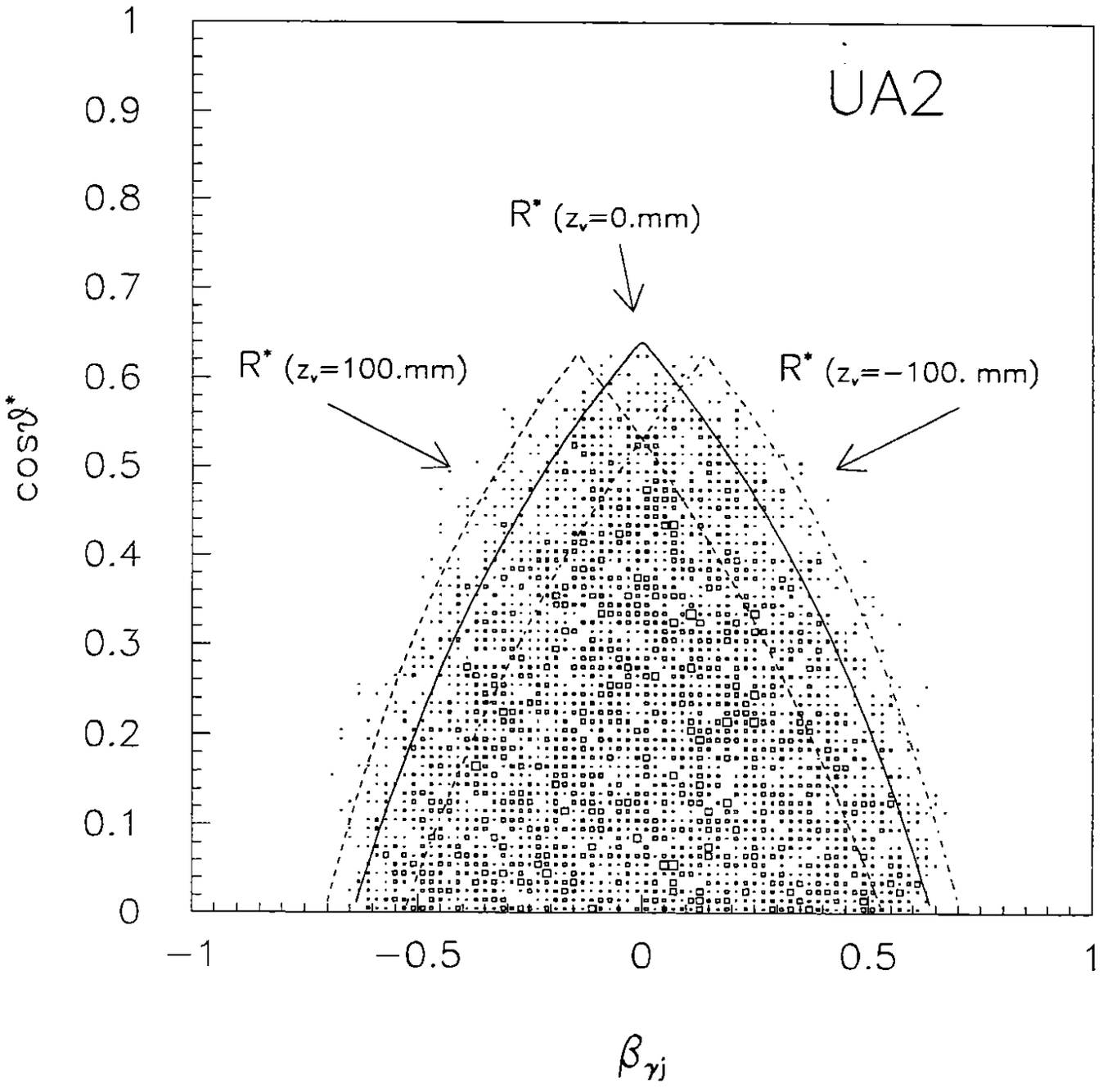
UA2
R* (z_v=0.mm)
R* (z_v=100.mm)
R* (z_v=−100. mm)
cosϑ*
β_γj
1
0.9
0.8
0.7
0.6
0.5
0.4
0.3
0.2
0.1
0
−1
−0.5
0
0.5
1

Fig. 1

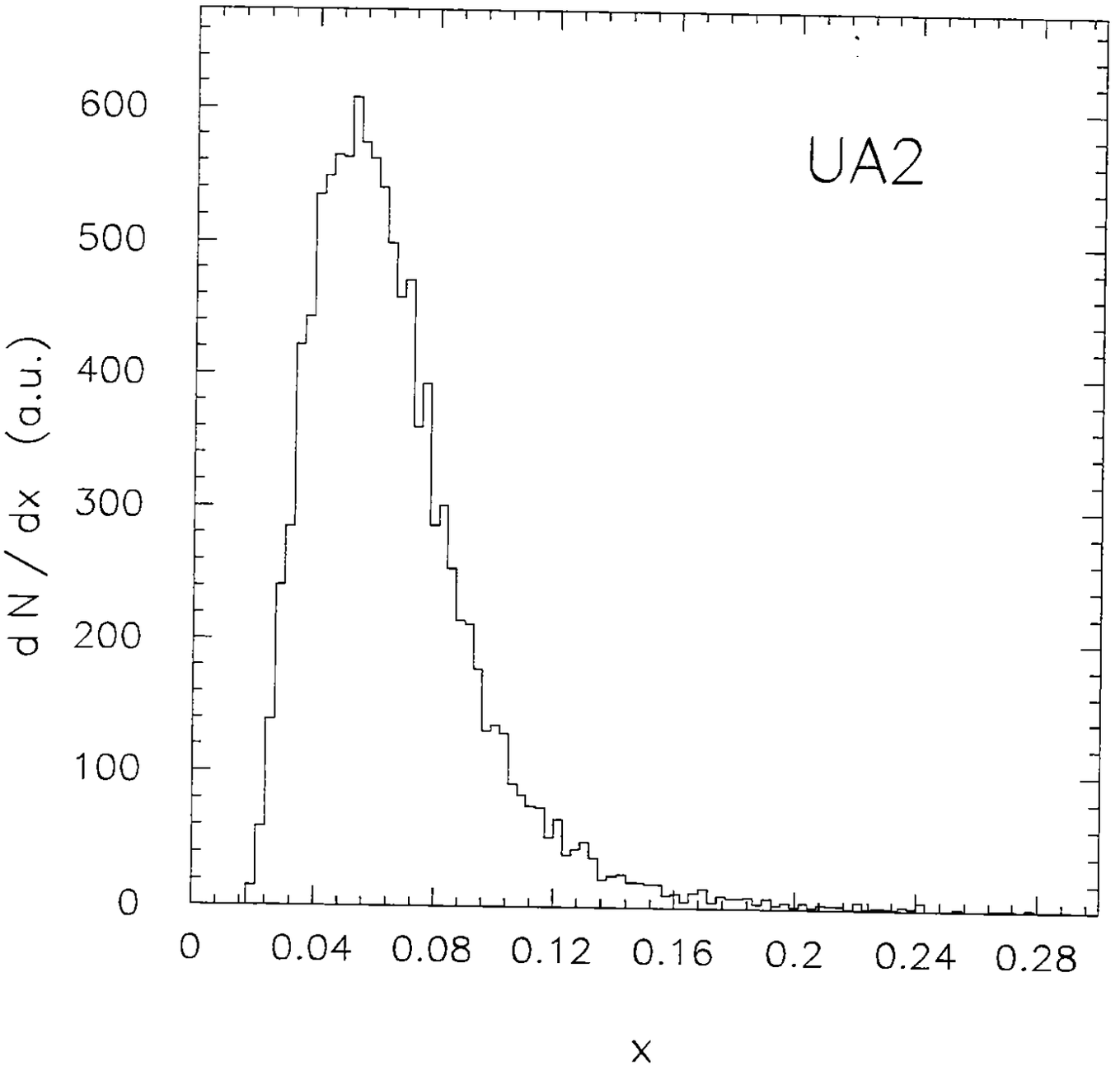
UA2
600
500
400
300
200
100
0
d N / dx (a.u.)
0
0.04
0.08
0.12
0.16
0.2
0.24
0.28
x

Fig. 2

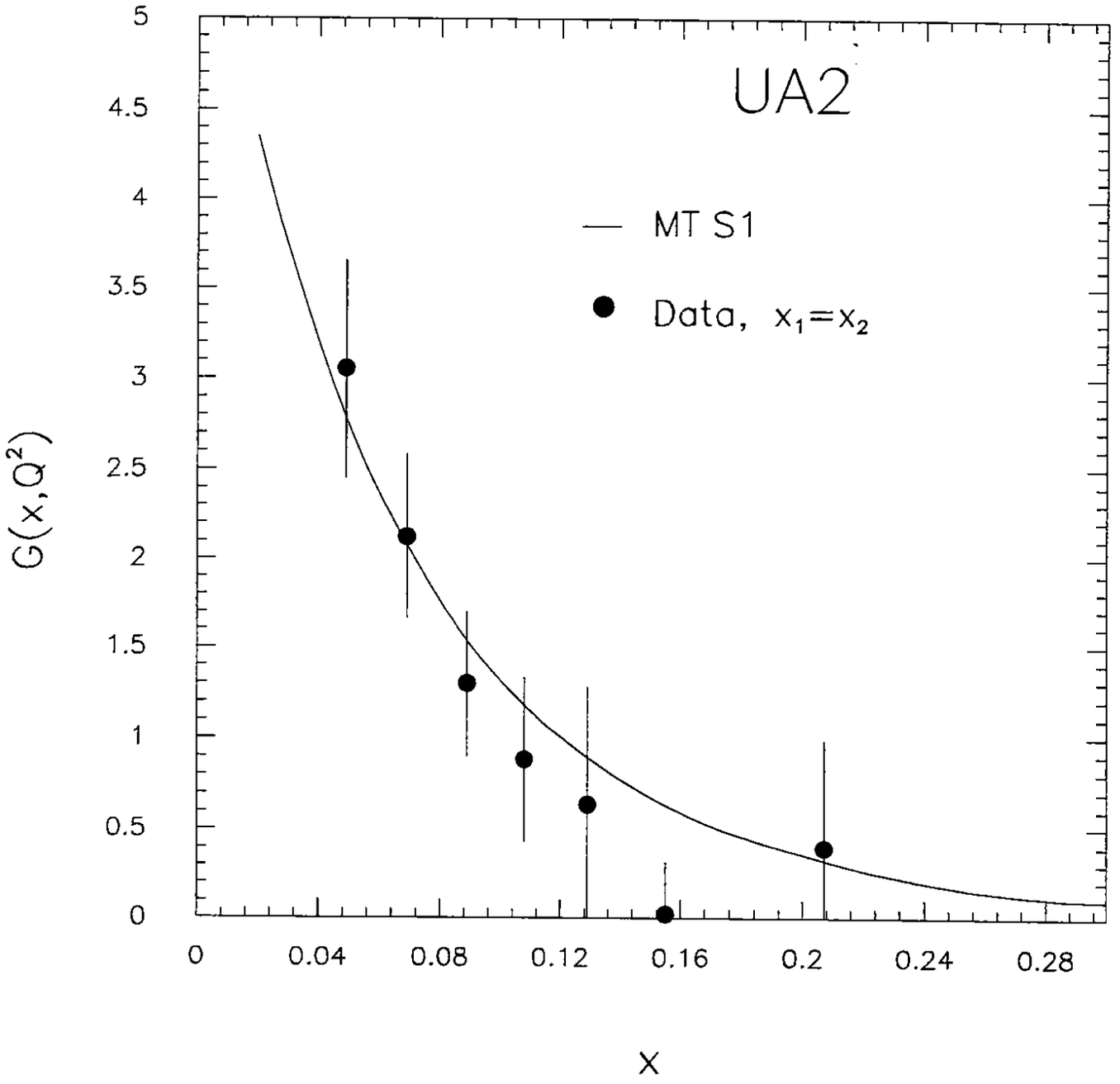
UA2
MT S1
Data, $x_1=x_2$
$G(x,Q^2)$
X
0
0.5
1
1.5
2
2.5
3
3.5
4
4.5
5
0
0.04
0.08
0.12
0.16
0.2
0.24
0.28

Fig. 3a

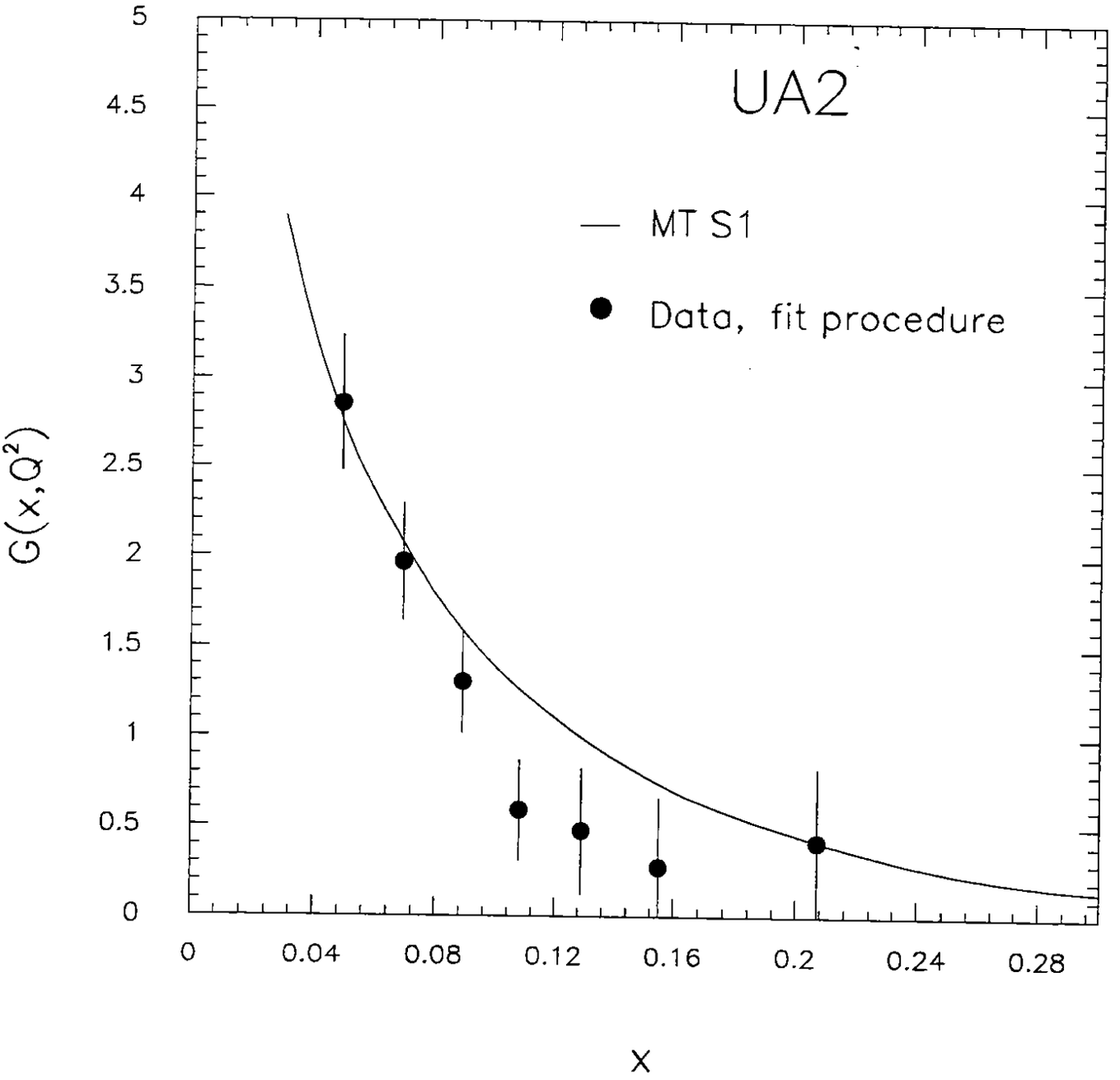
UA2
MT S1
Data, fit procedure
G(x,Q²)
X
5
4.5
4
3.5
3
2.5
2
1.5
1
0.5
0
0
0.04
0.08
0.12
0.16
0.2
0.24
0.28

Fig. 3 b

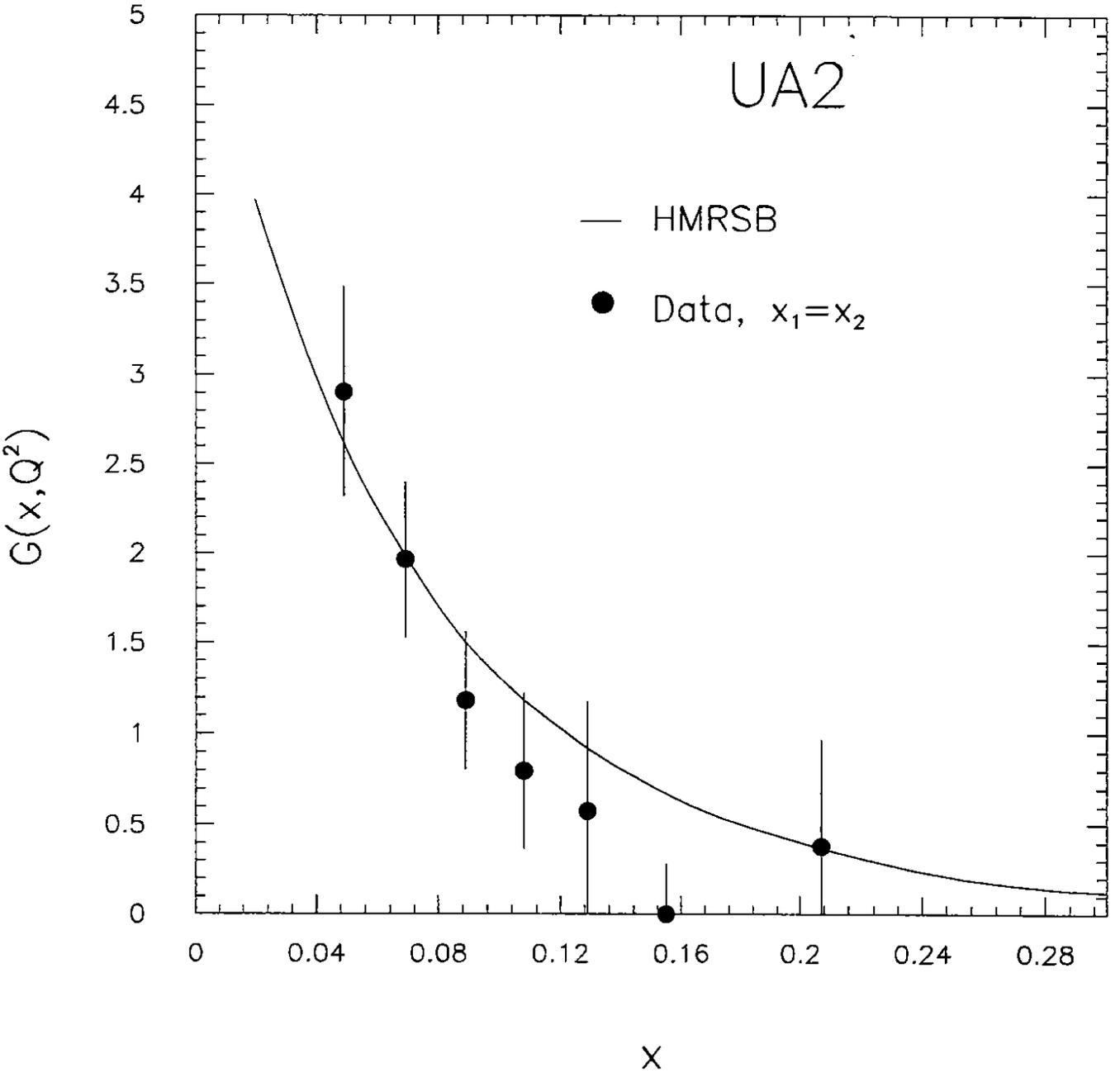
UA2
HMRSB
Data, $x_1=x_2$
$G(x,Q^2)$
X
0
0.5
1
1.5
2
2.5
3
3.5
4
4.5
5
0
0.04
0.08
0.12
0.16
0.2
0.24
0.28

Fig. 4 a

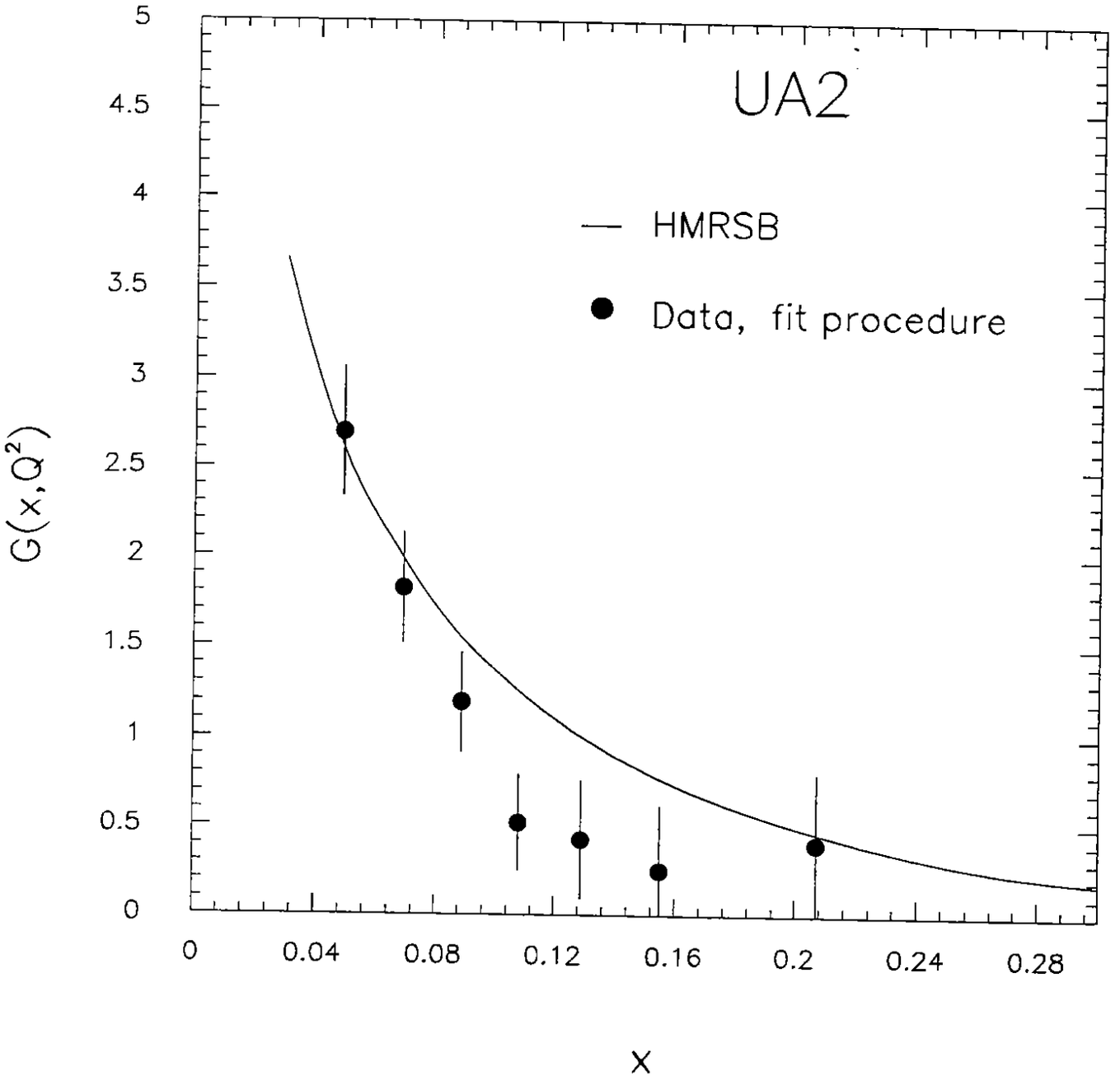
UA2
HMRSB
Data, fit procedure
G(x,Q²)
X
0
0.5
1
1.5
2
2.5
3
3.5
4
4.5
5
0
0.04
0.08
0.12
0.16
0.2
0.24
0.28

Fig. 4 b